Enhanced ~~i~~Internal ~~t~~Tidal ~~m~~Mixing in the Philippine Sea ~~m~~Mesoscale ~~e~~Environment

Jia You[1, 3, 4], Zhenhua Xu[*1, 2, 3, 4], Qun Li[5], Robin Robertson[6], Peiwen Zhang[1, 3, 4], Baoshu Yin[1, 2, 3, 4]

[1]CAS Key Laboratory of Ocean Circulation and Waves, Institute of Oceanology, Chinese Academy of Sciences, Qingdao, China

[2]Pilot National Laboratory for Marine Science and Technology, Qingdao, China

[3]Center for Ocean Mega-Science, Chinese Academy of Sciences, Qingdao, China

[4]College of Earth and Planetary Sciences, University of Chinese Academy of Sciences, Beijing, China

[5]Polar Research Institute of China, Shanghai, China

[6]China-Asean College of Marine Science, Xiamen University Malaysia, Sepang, Malaysia

Corresponding author: Zhenhua Xu, Institute of Oceanology, Chinese Academy of Sciences; Email: xuzhenhua@qdio.ac.cn.

Abstract.

Turbulent mixing in the ocean interior is mainly attributed to~~contributed by~~ internal wave breaking; however, the mixing properties and the modulation effects of mesoscale environmental factors are not well-known. Here, the spatially inhomogeneous and seasonally variable diapycnal diffusivities in the upper Philippine Sea were estimated from ARGO float data using a strain-based finescale parameterization. Based on a coordinated analysis of multi-source data, we found that the driving processes for diapycnal diffusivities mainly included the near-inertial waves and internal tides. Mesoscale features were important in intensifying the mixing and modulating its spatial pattern. One interesting finding was that, besides near-inertial waves, internal tides also contributed significant diapycnal mixing ~~for~~ in the upper Philippine Sea. The seasonal cycles of diapycnal diffusivities and their contributors differed zonally. In the mid-latitudes, wind-mixing dominated and was strongest in winter and weakest in summer. In contrast, tidal-mixing was more predominant in the lower-latitudes and had no apparent seasonal variability. Furthermore, we provide evidence that the mesoscale environment in the Philippine Sea played a significant role in regulating the intensity and shaping the spatial inhomogeneity of the internal tidal mixing. The magnitudes of internal tidal mixing w~~as~~ere greatly elevated in regions of energetic mesoscale processes. ~~The a~~Anticyclonic mesoscale features were found to enhance diapycnal mixing more significantly than ~~did~~ cyclonic ones.

Keywords: Mixing, Internal tides, Mesoscale, the Philippine Sea

1. Introduction

Turbulent mixing can alter both the horizontal and vertical distributions of temperature and salinity gradients. These then modulate the ocean circulation variability, both globally and regionally. Many studies have shown the existence of a complicated spatiotemporal pattern of diapycnal mixing in the ocean interior. Such mixing inhomogeneity can influence the hydrological characteristics, ocean circulation variability and climate change. The breaking of internal waves is believed to be the main contributor to the ocean's diapycnal mixing (eg. Liu et al., 2013, Robertson R., 2001). Thus, clear understanding of the spatial patterns and dissipation processes of broad-band internal waves is necessary to clarify and depict the global ocean mixing climatology.

The long-wavelength internal waves in the ocean ~~are~~occur mainly in the form of near-inertial internal waves (NIWs) and internal tides (eg. Alford and Gregg, 2001; Cao et al., 2018; Klymak et al., 2006; Xu et al., 2013), and the internal solitary waves evolved from them also can trigger mixing (eg. Deepwell et al., 2017; Grimshaw, et al., 2010; Shen et al., 2020). The wind-input NIW energy to the mixing layer is about 0.3-1.4 TW (eg. Alford, 2003; Liu et al., 2017; Rimac et al., 2013; Watanabe and Hibiya, 2002). The NIW energy propagate downward, mainly dissipate and drive energetic mixing within the upper ocean (Wunsch and Ferrari, 2004). Barotropic tidal currents flowing over rough topographic features can generate internal tides (eg. Robertson R., 2001; Xu et al., 2016), with the global energy of 1.0 TW (Egbert and Ray, 2001; Jayne and St. Laurent, 2001; Song and Chen, 2020). Near the generation sources, the internal tidal mixing intensify above the bathymetries, meanwhile, in the remote area, the tidal mixing ~~is~~ becomes distributed throughout the water column due to the multiple reflection and refraction processes. Therefore, the relative contributions to the upper-layer diapycnal diffusivities by NIWs and the spatial variability of internal tides ~~should differ regionally, which~~ deserves further investigation.

In mid-latitudes, NIWs dominate~~d~~ the upper ocean mixing, as a result of the presence of westerlies and frequent storms (eg. Alford et al., 2016; Jing et al., 2011; Whalen et al., 2018). However, from the global view, the upper ocean mixing geography is inconsistent with the global wind field distribution. For example, in low-latitudes, upper ocean mixing hotspots are located nearer to rough topographic features, regardless of the wind conditions. This indicates that upper ocean mixing might be attributed to non-wind-driven internal waves, such as internal tides. In order to better understand the ocean mixing patterns and modulation mechanisms, we need to clarify the relative contributions between the wind

62   and tidal energy.

63   Internal tides are generally considered to be important to ocean mixing in the deep ocean, be~~yond~~low

64   the influence of winds (Ferrari and Wunsch, 2009; Munk et al., 1998; MacKinnon et al., 2017). Many

65   factors influence the spatial pattern and energy transfer of internal tides. Higher-mode internal tides break

66   more easily near their sources, while the low-mode internal tides propagate long distances, even

67   thousands of kilometers. Propagating internal tides will be limited by several factors, such as topography,

68   stratification and turning latitude (eg. Vlasenko et al., 2013; Song and Chen, 2020; Hazewinkel &

69   Winters, 2011). Wave-wave interaction in the ocean also influences the spatiotemporal variability of

70   internal tides. For example, PSI (parametric subharmonic instability) is a potential avenue to transfer

71   internal tidal energy to other frequencies (Ansong et al., 2018). Moreover, stratification and background

72   flows also contribute to internal tidal spatial and temporal variability (eg. Karry et al., 2016; Huang et

73   al., 2018; Chang et al., 2019). Due to the complicated multi-scales of the background flows, it is still

74   unclear about how the background flow modulates the internal tides, their energy dissipation and ocean

75   mixing.

76   Recent research suggests that the mesoscale environment is a key factor influencing ocean mixing.

77   There is evidence that mesoscale eddies can enhance wind-driven mixing and internal tidal dissipation.

78   This enhancement will be more significant in the presence of an anticyclonic eddy (eg. Jing et al., 2011;

79   Whalen et al., 2018). Likewise, regional studies indicate that mesoscale features modulate the generation

80   and propagation of internal tides. Mesoscale currents can also broaden the range undergoing internal tide

81   critical latitude effects and enhance the energy transfer from diurnal frequencies to semidiurnal or high

82   frequencies (Dong et al., 2019). Mesoscale eddies are found to modulate internal tide propagation

83   (Rainville and Pinkel, 2006; Park and Watts, 2006; Zhao et al., 2010) and enable the internal tide to lose

84   its coherence (Nash et al., 2012; Kerry et al., 2016; Ponte and Klein, 2015). Numerical simulation results

85   support these observations (Kerry et al. 2014), indicating that the patterns of internal tides ~~is~~ are largely

86   modulated by the position of eddies. An idealized numerical experiment shows that the energy of internal

87   tides shows bundled beams after passing through an eddy (Dunphy and Lamb, 2014). And the mode-1

88   internal tid~~ales~~al interactions with eddies will trigger higher-mode signals. Up to now, research ~~about~~on

89   mesoscale–internal tide interactions has been ~~been~~ primarily focused on the propagation pattern or 3-D

90   structure of internal tides and has ignored their energy dissipation and mixing effects. The latter ~~is~~are

91   more important for ~~altering~~impacts on the ocean circulation variability and climate change.

92   The Philippine Sea, located in the Northwestern Pacific Ocean, is one of the most energetic internal

93   tidal regimes in the world. In this region, powerful internal tides significantly enhance ocean mixing, as

94   shown by numerical simulations (Wang et al., 2018). The importance of sub-inertial shear to ocean

95   mixing has been hypothesized from observations (Zhang et al., 2019), and the importance of internal

96   tides to mixing is supported through parameterization techniques (Qiu et al., 2012). On the other hand,

97   the Philippine Sea is an area with frequent typhoons, which make significant contributions to ocean

98   mixing. Consequently, ~~M~~multiple factors and mechanisms impact the turbulent mixing distribution in

99   the Philippine Sea (Wang et al., 2018). To date, it is unclear what the dominant factors are and how these

100   factors modulate the ocean mixing properties. Moreover, the role of mesoscale environment in regulating

101   ocean mixing is still not well understood.

102   ~~At p~~Presently, coupled numerical models are basically able to accurately simulate the generation and

103   propagation of internal tides. The internal tide dissipation and induced mixing are found to be important

104   for the determination of correct mixing parameterizations in numerical models (Robertson and Dong,

105   2019). Some existing studies focus on the simulations of internal tidal breaking and tidally induced

106   mixing (Kerry et al., 2013; Kerry et al., 2014; Muller, 2013; Wang et al., 2018). It is difficult to provide

107   a complete spatial and temporal picture from direct observations of turbulence. This is due to the scarcity

108   of observations and their patchy distribution in time and space. Multisource data covering multiple tidal

109   cycles or preferably a spring-neap cycle, as well as a broad domain, are necessary to acquire the

110   spatiotemporal distribution and few of these have been collected. The development and application of

111   parameterization methods provide greater possibility of characterizing a broad-regional mixing

112   distribution and variability. A global pattern of ocean mixing has been provided using these

113   parameterization methods (Whalen et al. 2012; Kunze 2017). Furthermore, sensitivity studies have been

114   performed investigating the dependence of several factors to global mixing, such as bottom roughness,

115   internal tides, wind and background flows (eg. Whalen et al. 2012; Waterhouse. 2014; Kunze and Eric.

116   2017; Whalen et al. 2018; Zhang et al. 2019). At present, parameterization is the most effective method

117   to investigate the modulation of tidal mixing by mesoscale background flows.

118   The spatial pattern and temporal variability of diapycnal diffusivities in the Philippine Sea are

119   examined in this paper. We provide evidence to verify the importance of tidal mixing in the upper layer

120   of this region. Moreover, we illustrate the modulation of mesoscale environment in tidal mixing

121 properties and distributions. Our data and methods are detailed in Section 2. Results and analysis,

122 including the spatial patterns and seasonal cycle of mixing, contributions of influencing factors and

123 internal tide-mesoscale interrelationships, are shown in Section 3. Finally the summary and discussion

124 are given in Section 4.

2. Method and Data

2.1 ARGO and Fine-scale parameterization method

127 The ARGO Program is a joint international effort involving more than 30 countries and organizations

128 and having deployed over 15,000 freely drifting floats since 2000. The accumulated total of collected

129 profiles exceeds 2 million profiles of eConductivity, tTemperature, dDepth (CTD) along with other

130 geobiochemical parameters. The ARGO program has become the main data source for many research

131 and operational predictions of oceanography and atmospheric science (http://www.ARGO.ucsd.edu). We

132 screened the profiles from the Philippines Sea with quality control and estimated diapycnal diffusivity

133 and dissipation rate from them using a finescale parameterization.

134 The diapycnal diffusivity and turbulent kinetic energy dissipation rate can be estimated from a fine-

135 scale strain structure. This is based on a hypothesis that the energy can be transported from large to small

136 scales. In such scales, waves break due to shear or convective instabilities by weakly nonlinear

137 interactions between internal waves (Kunze et al., 2006). Presently, this method has been widely used

138 for the global ocean (eg. Wu et al., 2011; Kunze et al., 2017; Whalen et al., 2012; Fer et al., 2010;

139 Waterhouse et al., 2014). The dissipation rate ε can be expressed as

$$\varepsilon = \varepsilon_0 \frac{\overline{N^2}}{N_0^2} \frac{\langle \xi_z^2 \rangle^2}{\langle \xi_{z\,GM}^2 \rangle^2} h(R_\omega) L(f, \overline{N}) \tag{1}$$

141 where $\varepsilon_0 = 6.73 \times 10^{-10} W/kg$ and $N_0 = 5.24 \times 10^{-3}/s$, and $\overline{N^2}$ represents the averaged buoyancy

142 frequency of the segment. $\langle \xi_{z\,GM}^2 \rangle$ and $\langle \xi_z^2 \rangle$ are strain variance from the Garrett-Munk (GM) spectrum

143 (Gregg and Kunze, 1991) and the observed strain variance, respectively. The angle brackets indicate

144 integration over a specified range of vertical internal wavenumbers (see equations 4 and 5). The function

145 $h(R_\omega)$ accounts for the frequency content of the internal wave field and R_ω represents shear/strain

146 variance ratio. R_ω is fixed at 7, which is a global mean value (Kunze et al., 2006).

$$h(R_\omega) = \frac{1}{6\sqrt{2}} \frac{R_\omega(R_\omega + 1)}{\sqrt{R_\omega - 1}} \tag{2}$$

148   The function $L(f,\overline{N})$ corrects for a latitudinal dependence, here f is the local Coriolis frequency,

149 and f_{30} is the Coriolis frequency at $30°$, and $\overline{N}$ is the vertically averaged buoyancy frequency of the

150 segment.

$$L(f,\overline{N}) = \frac{f\,arc\text{cr}cosh(\frac{\overline{N}}{f})}{f_{30}\,arc\text{cr}cosh(\frac{\overline{N}}{f_{30}})} \tag{3}$$

152 strain ξ_z was calculated from each segment,

$$\xi_z = \frac{N^2 - N_{ref}^2}{\overline{N^2}} \tag{4}$$

$$\langle\xi_z^2\rangle = \int_{k_{min}}^{k_{max}} S_{str}(k_z)dk_z \leq 0.2 \tag{5}$$

155   We derived N from 2 to 10 dbar-processed temperature, salinity, and pressure data according to the

156 ARGO float resolution. N_{ref}, as a smooth piece-wise quadratic fit to the observed N profile, is fitted to

157 24 m. Here we remove segments that vary in the range of $\langle N^2\rangle > 5 \times 10^{-4}s^{-2}$ or $\langle N^2\rangle < 1 \times$

158 $10^{-9}s^{-2}$ since the strain signal at these levels is dominated by noise (Whalen et al., 2018). By applying

159 a fast Fourier transform (FFT) on half-overlapping 256 m segments along each vertical ξ_z profile, we

160 computed the spectra $S_{str}(k_z)$ and integrated them to determine the strain variance. We integrated these

161 spectra between the vertical wavenumbers $k_{min} = 0.003\ cmp$ and $k_{max} = 0.02\ cmp$ according to

162 typical global internal tideal typical scales and equation 5, respectively. Substituting $\langle\xi_z^2\rangle$into equation

163 (1) ultimately yields 32 m resolved vertical profilessections of each observed profiles.   The dissipation

164 rate ε is related to the diapycnal diffusivity K_z by the Osborn relation

$$K_z = \Gamma\frac{\varepsilon}{\overline{N^2}} \tag{6}$$

166 where the flux coefficient Γ is fixed at 0.2 generally.

167

168 **2.2 ERA-Interim and Slab-model**

169   The near-inertial energy flux for each observation profile was calculated using the 10 m wind speed

170 product from ERA-Interim (https://www.ecmwf.int/en /forecasts/datasets), which is 6-hourly wind speed

171 on a grid of $0.75°\ \times0.75°$. We selected the mean near-inertial flux of 30-50 days before the time of

172 each diapycnal diffusivity estimation as our measure of the near-inertial flux, with the consideration of

173 the propagation of NIWs.

174   The wind-drive NIW energy flux can be directly estimated using a slab model, which assumes that the

175   inertial oscillations in the mixed layer do not interact with the background fields. The mixed layer current

176   velocity can be described by

177   $$\frac{dZ}{dt} + (r + if)Z = \frac{T}{\rho H}$$ (7)

178   where $Z = u + iv$ is the mixed layer oscillating component of full current, and i is an imaginary

179   number to indicate the latitudinal component. $T = (\tau_x + i\tau_y)$ is the wind stress on the sea surface, f

180   is the local Coriolis parameter, r is the frequency-dependent damping parameter, which was fixed

181   at $0.15 f$ for these calculations. ρ is sea water density and fixed at 1024 kg/m^3. H is the mixed-layer

182   depth and was set to a constant 25 m. We can calculate the oscillating component of full velocity from

183   equation 7 and obtain the near-inertial component through a bandpass filter of [0.85, 1.25] f. The near-

184   inertial energy flux is calculated as

185   $$EH(\Pi) = Re(Z \cdot T^*)$$ (8)

186   the asterisk (*) indicates the complex conjugate of a variable.

2.3 AVISO and Eddy kinetic energy

188   The eddy kinetic energy is estimated based on geostrophic calculation as:

189   $$EKE = \frac{1}{2}\left(U_g'^2 + V_g'^2\right)$$ (9)

190   $$U_g' = -\frac{g}{f}\frac{\Delta\eta'}{\Delta y} \qquad V_g' = -\frac{g}{f}\frac{\Delta\eta'}{\Delta x}$$ (10)

191   where U_g' and V_g' are the geostrophic velocities in the east-west and north-south directions,

192   respectively. They are taken from the AVISO (http://www.aviso.altimetry.fr/duacs/) geostrophic velocity

193   product. η' indicates sea level anomaly (SLA).

2.4 Internal tidal conversion rates

195   The internal tidal conversion rate was provided by SEANOE (https://www.seanoe.org/data/, C.de

196   Lavergne et al., 2019), including 8 main tidal constituents. We used the mode-summed internal tidal

197   conversion rates of M_2 and K_1, and integrated 8 main tidal constituents in present study.

3. Results

3.1 Spatial pattern of diapycnal mixing in the upper Philippine Sea

200   The diapycnal diffusivities were used as indicators of ocean diapycnal mixing. The pattern averaged

201   within 250-500 m is shown in Fig.1a. The K_z was estimated from the ARGO profiles, with an average

202 on each cell of 0.5°×0.5°. The magnitude of diapycnal diffusivities increased with latitude, reaching *10*-

203 *⁴ m²s⁻¹* in the northern part of this area (30°N-36°N). The mean value of K_z was about O(-6)-O(-5) in

204 lower latitude. While, it was remarkable that the magnitude of K_z also increased significantly in some

205 low-latitude regions, reaching O(-4) or higher. ~~These regions include Izu Ridge (Nagasawa et al., 2005;~~

206 ~~Tanaka et al., 2018) and~~ , such as Luzon Strait (Xu et al., 2014). Reviewing the influence of topography,

207 wind and internal tide (Fig.1b-d) on ocean mixing, it was found that the latitudinal~~zonal~~ variability of

208 K_z was consistent with the wind intensity distribution. Upper ocean mixing was significantly enhanced

209 at mid-latitudes due to the presence of westerlies. In addition, K_z was also enhanced near several key

210 internal tide sources, such as the Luzon Strait, Bonin Ridge, Izu Ridge, Dadong Ridge, etc. At these sites,

211 the magnitude of K_z was obviously larger than other areas at the same latitude, indicating a significant

212 role of internal tides. Additionally, the enhancement of deep ocean mixing at these sites was even more

213 obvious (not shown).

214
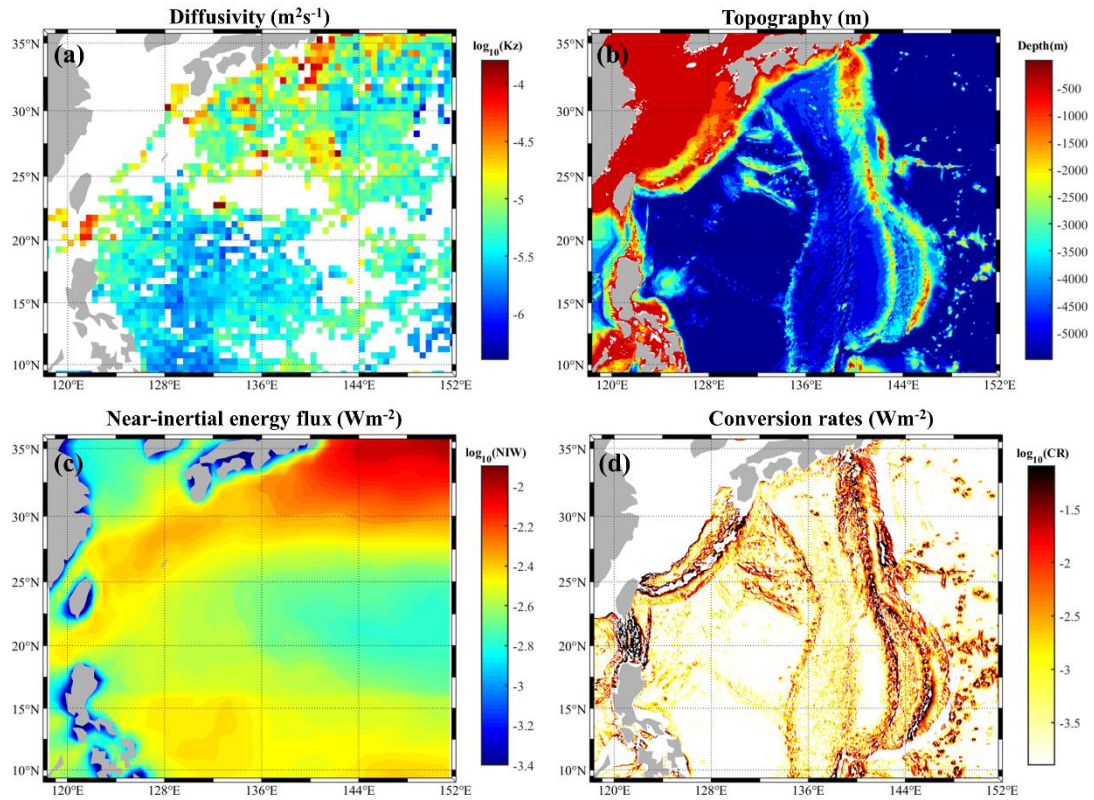
215 **Figure 1 Maps of (a) log-scale averaged diapycnal diffusivities K_z (m²s⁻¹) estimated from ARGO profiles,**

216 **(b) topography, (c) log-scale long-term averaged near-inertial energy flux from wind (Wm⁻²), and (d) log-scale**

217 **M2 internal tide conversion rates (Wm⁻²).**

218

219 It can be noted that the pattern of diapycnal diffusivities was not completely consistent with those of

220 either internal tides or winds. This suggests that the ocean mixing was modulated by other factors than

221 tides and winds. The magnitudes of K_z also vary for internal tide source sites. Considering that the

222 Philippine Sea is a region with energetic mesoscale motions (Fig.2), the influences of mesoscale features

223 in turbulent mixing should be taken into account. The existence of mesoscale features can alter the

224 propagation and dissipation of internal tides. Therefore, the Philippine Sea is an ideal region to study the

225 modulation of background flows on turbulent mixing associated with strong internal tides.

226
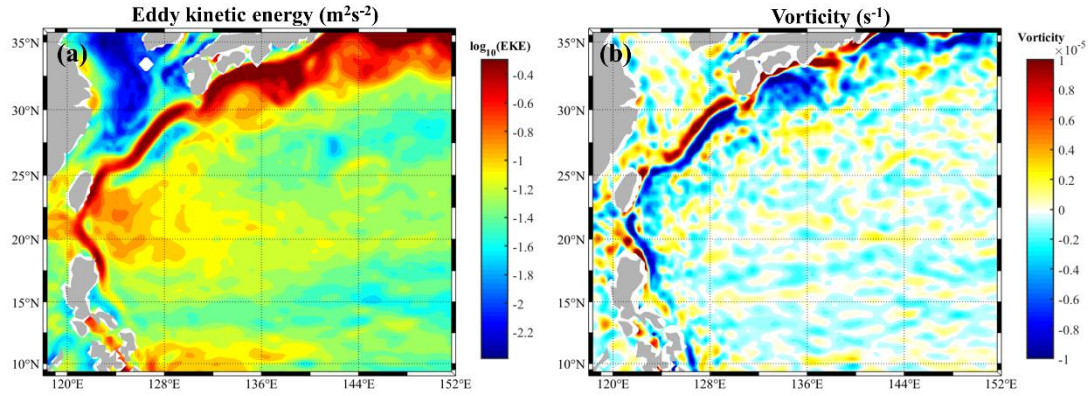
227 **Figure 2 Maps of (a) log-scale long-term averaged eddy kinetic energy and (b) long-term averaged vorticity.**

228

229 **3.2 Seasonal variability of mixing at different latitudes**

230 The seasonal cycle for diapycnal diffusivities also differs zonally. Here, we divided the Philippine Sea

231 into two portions: low-latitude (10°N-25°N) and mid-latitude (25°N-35°N). The diapycnal diffusivities

232 K_z were averaged in each latitude band (Fig.3). At the depth of 250-500 m in the mid-latitude, the

233 diapycnal diffusivities had a significant seasonal trend as strong in winter and weak in summer. This is

234 consistent with the seasonal fluctuation of near-inertial energy from wind. Such a seasonal cycle could

235 also be found at 500-1000 m and 1000-1500 m in the mid-latitudes, but it was relatively weaker,

236 especially after 2016. In the lower latitudes, the NIW energy was still strong in winter and weak in

237 summer, but a seasonal dependence of turbulent mixing was not obvious, even in the upper ocean.

238 Consequently, the wind was found to play a significant role in driving turbulent mixing at mid-latitude,

239 but was insignificant at low latitudes. Other factors drove and modulated turbulent mixing in low

240 latitudes.

241
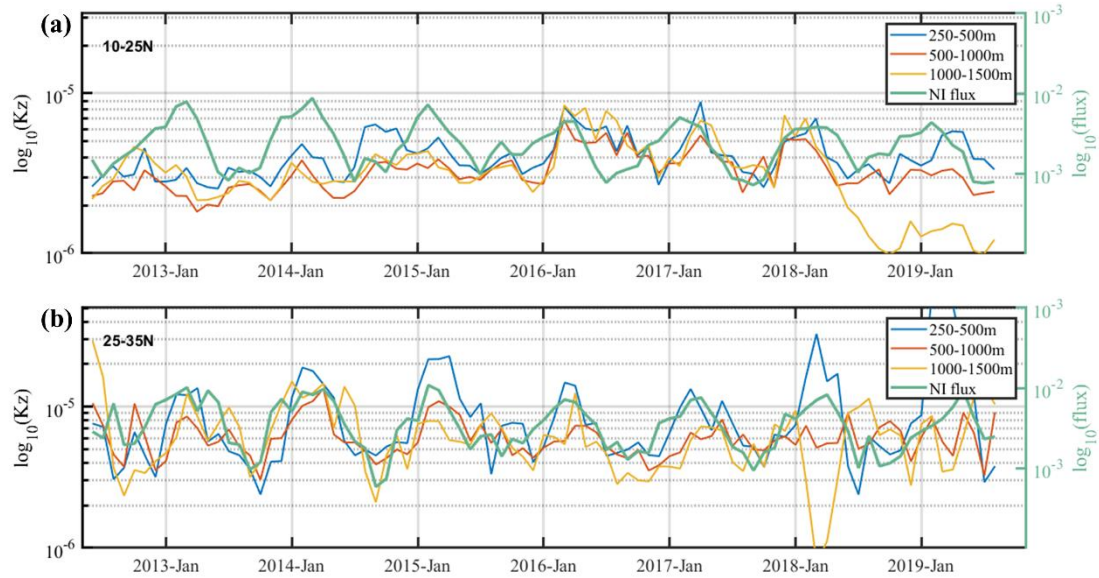
Figure 3 Seasonal cycles in diapycnal diffusivities (colorful line) and near-inertial energy flux from wind
(green) extents to 250-500 m, 500-1000 m and 1000-1500 m in (a) 10°N -25°N and (b) 25~~10~~°N-35~~25~~°N, which
is averaged in each month and all water column.

3.3 Impact factors

3.3.1 Relative contributions

The turbulent mixing of the Philippine Sea displayed an obvious ~~latitudinal~~latitudinal dependence, so

the latitudinal influence was examined for several factors: internal tides, wind and eddy kinetic energy

(Fig.4).

~~The diapycnal diffusivities in the regions of weak internal tides and strong internal tides were averaged~~

~~in each 1° latitude band.~~ Each 1°latitude band was separated into two regions with weak or strong internal

tides (or other factors). Here we d~~i~~efine the strong or weak internal tides as the internal tide conversion

rate larger or smaller than the median of the Philippine Sea. The diapycnal diffusivities in these two kinds

of regions were then averaged. The similar method has been used to analyze the effect of topography and

different frequency-bands internal waves on ocean interior shear and mixing (eg. Whalen et al., 2012;

Zhang et al., 2019).~~A similar method has been used to analyzed the effect of topography or different~~

~~frequency bands waves on mixing (eg. Whalen et al., 2012; Zhang et al., 2019).~~ For a more direct

representation, the ratios of diapycnal diffusivities above the strong internal tides to weak internal tides

were shown.~~The ratio of diapycnal diffusivities above the strong internal tides to weak internal tides are~~

~~shown.~~ The ratio larger than 1 means that the diapycnal diffusivities are significantly higher in the regions

262 of strong internal tides. ~~This ratio larger than 1 means that the diapycnal diffusivities is higher in the~~

263 ~~regions of strong internal tides than above weak internal tide in this latitudinal band.~~ The larger this ratio

264 is ,the more important the internal tid~~e~~al induced mixing. Similarly, the contributions of near-inertial

265 wave and eddy kinetic energy ~~are~~were analyzed ~~in~~by this statistical method. The strong near-inertial

266 wave or eddy kinetic energy is the locations where this parameter exceeds the regional median.

267 ~~The rates of diapycnal diffusivities in regions of weak/strong internal tides, weak/strong NIW energy,~~

268 ~~and high/low eddy kinetic energy were calculated in each 1° latitude, respectively. If the rate was close~~

269 ~~to 1, the influence of this factor was insignificant, while a larger rate indicated a greater contribution.~~

270
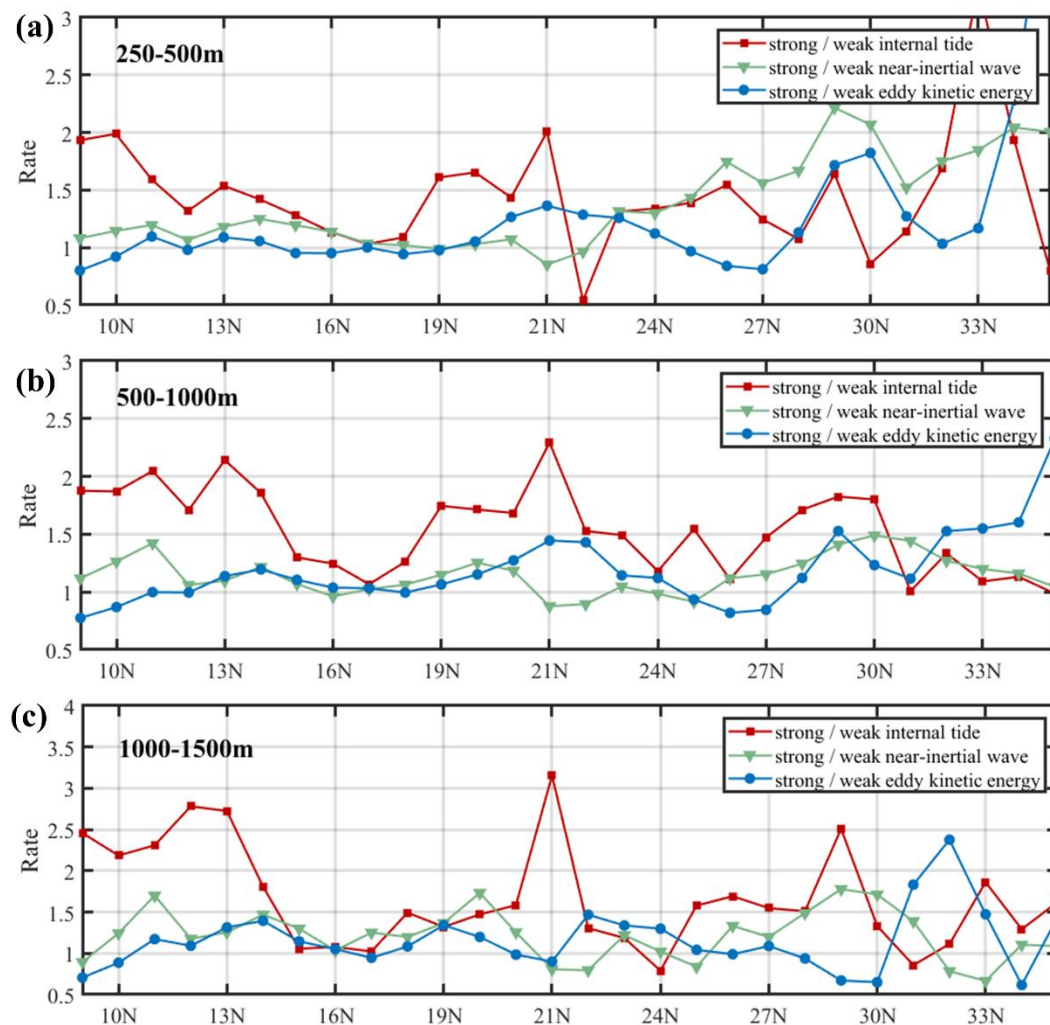
271 **Figure 4 Ra~~te~~tios of diapycnal diffusivities between areas over strong (greater than median) and weak internal**

272 **tide (red lines), strong (greater than median) and weak near-inertial wave (green lines) and strong (greater**

273 **than median) and weak eddy kinetic energy (blue lines) for each 1° latitude bands in the depth range of (a)**

274 **250-500 m, (b) 500-1000 m and (c) 1000-1500 m, Which averages for each bands containing more than 10**

275 **estimates.**

276

277   At depths of 250-500 m, the ratio~~rate~~ associated with internal tide increased significantly at 10°N,

278 21°N and 33°N. These latitudes correspond to Guap seamount, Luzon Strait and Izu Ridge, which are

279 main internal tid~~e~~al source sites. It reached 2 near these three latitudes, indicating that strong internal

280 tides triggered the enhancement of K_z twice as much compared to the regions of weak internal tides. In

281 addition, north of 2~~3~~3°N, the ~~rate~~ratio in related to NIW in the upper ocean increased significantly with

282 latitude~~.~~. ~~And it exceeded the internal tidal contribution north of 25°N,~~ which indicated that the wind

283 plays a more important role in mixing at this latitude band. This result~~s~~ is basically consistent with ~~the~~

284 previous studies (Whalen et al., 2018), which suggested that the mixing is dominated by wind ~~–~~in the

285 mid-latitude. Taking the wind as the driving factor better explains the seasonal cycle of diapycnal

286 diffusivities in Fig.3, since the winds have an apparent seasonal dependence. The obvious seasonal trend

287 of K_z due to the important contribution of wind occurs between 25°N-35°N. In contrast, the ~~rate~~ratio

288 for wind is ~1 at lower latitudes, indicating that the wind-driven mixing is insignificant here with the

289 absence of wind-driven seasonal cycle.

290   The ~~contribution of~~ wind contribution to turbulent mixing is significantly reduced in the depth ranges

291 of 500-1000 m and 1000-1500 m (Fig.4 b and c). The ratio~~rate~~ only increased slightly at mid-latitudes,

292 less than 2 anywhere. In contrast, the enhancement of mixing triggered by internal tides at these depth

293 ranges was more significant, with the ratio~~rate~~s exceeding 3.5 at some latitudes. This suggested that

294 internal tides played a more important role in deep ocean mixing. Furthermore, internal tides significantly

295 enhanced K_z around 13°N, 21°N, and 29°N, corresponding to the sources of Mariana Trench, Luzon

296 Strait and Bonin Ridge, respectively. Such enhancement was not obvious at the Izu Ridge possibly due

297 to the shallower depth and paucity of deep data, or the turning latitude effects in this area.

298   Combined with the analysis of relative contributions of different factors in different layers, it was

299 concluded that the contribution of internal tides in turbulent mixing is more important in low latitudes of

300 the Philippine Sea. In this area, the wind and mesoscale features did not significantly enhance K_z. At

301 mid-latitudes, internal tides still played an important role, but the wind contribution was more significant

302 in the upper ocean. The wind drove turbulent mixing even at the depths of 500-1000 m and 1000-1500

303 m. The mid-latitude region not only corresponds to westerlies, but also features energetic mesoscale

304 motions. Therefore, the mesoscale features might be a potential factor for the enhanced turbulent mixing.

305 The modulation of mesoscale environment~~s~~ in the wind-induced mixing are discussed by some previous

306 studies (eg. Jing et al., 2011; Whalen et al., 2018), while the impact of mesoscale~~s~~ features in tide-induced

307   mixing and in lower latitudes ~~are~~were not be considered.

308   The Philippine ~~s~~Sea ~~are~~was separated ~~to~~into two latitude bands. The vertical structures of diapycnal

309   diffusivities in the regions with strong ~~and~~or weak internal tides ~~are~~were compared (Fig.5). This result

310   can directly reveal the enhancement of internal tide on mixing at different depths. ~~The~~A similar analysis

311   ~~are~~was used for wind and EKE. In the low latitudes, K_z did not increase in the regions of high eddy

312   kinetic energy or strong near-inertial energy, whereas, it increased significantly in the regions of strong

313   internal tides. This enhancement was more obvious below 400 m (Fig.5 a). And in the mid-latitudes, K_z

314   in the upper ocean increased significantly corresponding to strong winds with compared to weak winds

315   (Fig.5 b). Meanwhile, K_z was also larger in the regions of strong internal tides and high EKE in the

316   upper ocean. The enhancement of wind or EKE to turbulent mixing significantly weakened below 600

317   m, while the enhancement of internal tides increased with depth. Here, these results convey~~s~~ several

318   information: 1. Wind and EKE play~~s an~~ important roles on mixing in the upper ocean in the middle

319   latitudes; 2. Strong internal tide~~s is easier to~~facilitate and enhance mixing in the deeper ocean. These two

320   conclusions ~~is~~are consistent with previous researchers (eg. Jing et al., 2011; Whalen et al., 2012;

321   Waterhouse et al., 2014; Mackinnon et al., 2017; Whalen et al., 2018~~-~~). ~~This~~In addition, our results

322   indicate~~s~~ that, in the Philippine Sea, internal tides play~~ed~~ a significant role in turbulent mixing not only

323   in the low latitudes, but also in the mid latitudes,and not only in the deeper ocean, but also in the upper

324   ocean. ~~with their strong winds.~~

325
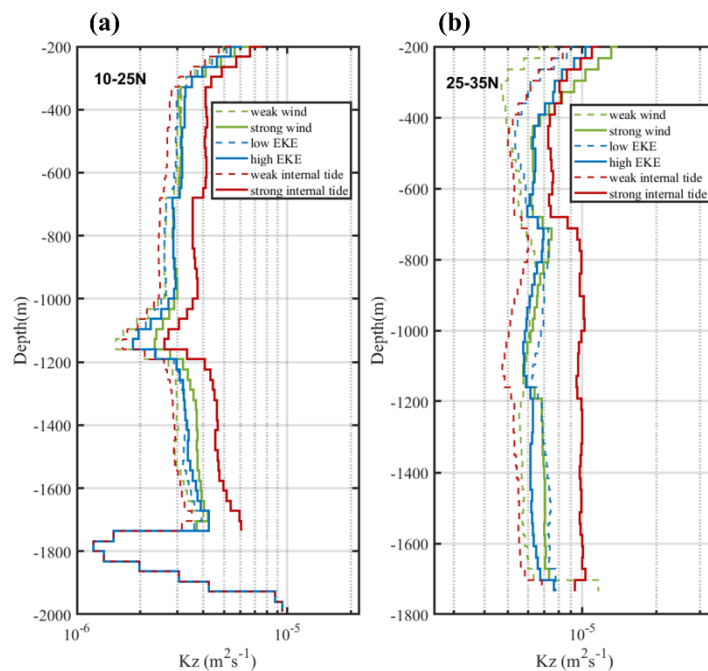
Figure 5 Vertical structures of geometric averaged diapycnal diffusivities K_z with weak and strong wind (green), low and high EKE (blue) and weak and strong internal tide (red) in the (a) low-latitude and (b) middle latitudes.

3.3.2 Wind

We adopted the linear regression approach and obtained the correlation between diapycnal diffusivities and wind. This approach is generally used to statistics the correlation between two factors (eg. Wu et al., 2011; Jing et al., 2014; Jeon et al., 2018; Zhao et al., 2019). The ~~least squares linear fit slopes~~regression coefficient is able to ~~of K_z to NIW energy from wind~~ represent the mixing response to wind (eg. Qiu et al., 2012). Here, the Philippine Sea is divided into 10°~~N 15°N, 15°N~~-25°N and 25°N-35°N (Fig.6). At the depth of 250-500 m, the slope is ~~the larges~~significant large~~er~~t in 25°N-35°N (~0.305), ~~followed by that in 10°N 15°N (~0.133),~~ and ~~the~~ small~~er~~est in 1~~5~~0°N-25°N (~0.0~~13~~29). The wind driven turbulent mixing was most significant between 25 °N-35 °N, but was insignificant between 1~~5~~0°N-25°N. At the depth of 500-1000 m, the wind influence on turbulent mixing was weakened in the mid-latitudes. This was consistent with the results of Fig.3 and Fig.4. It proved that the contribution of wind has a latitudinal~~zonal~~ dependence, which was significant at the mid-latitudes, but insignificant at low latitudes. In addition, the response of turbulent mixing to wind weakened quickly with depth, indicating that the dominant factor of mixing in the deeper water column was not wind. Accordingly, it was difficult for wind to drive mixing below 1000 m, so we do not show the results at the depth of 1000-1500 m (Fig.4).

345
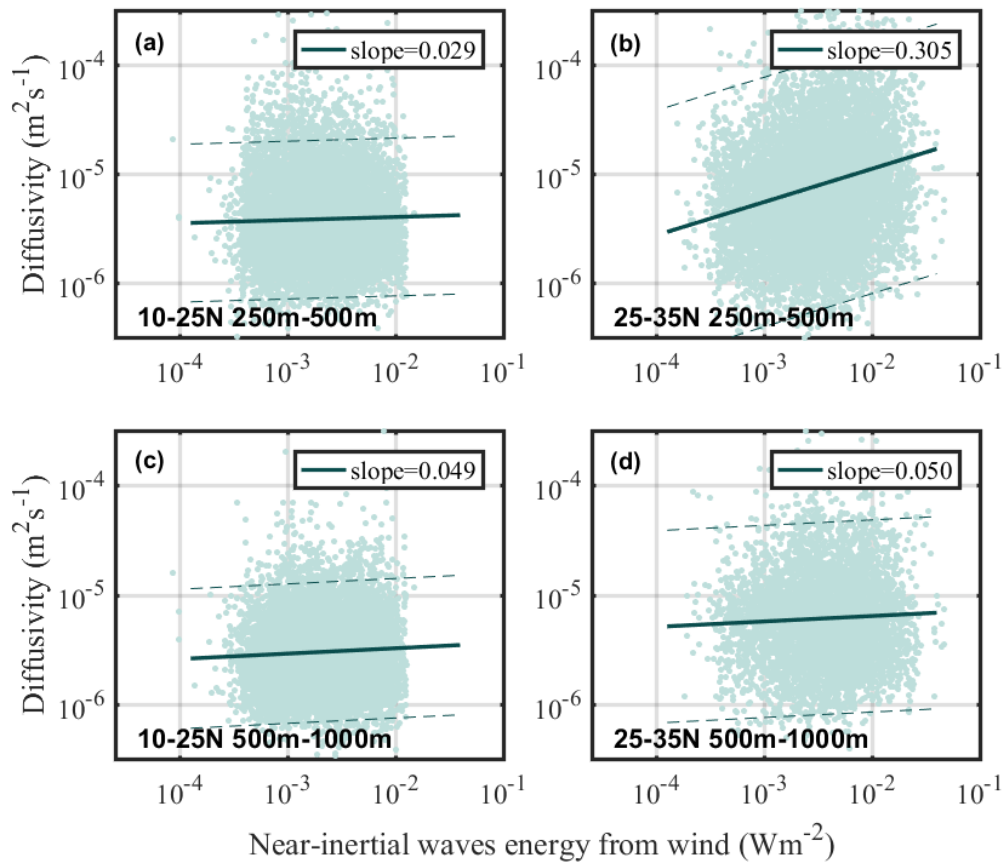
346 **Figure 6 Scatter of log-scale Kz versus log-scale near-inertial energy flux from wind in 250-500 m between (a)**

347 **10°N -~~1~~25°N ~~, (b) 15°N-25°N~~ and (e~~b~~) 25°N-35°N, and in 500-1000 m between (~~d~~c) 10°N-~~1~~25°N ~~, (e) 15°N-25°N~~**

348 **and (~~f~~d) 25°N-35°N The best-fit slopes are denoted by the solid line~~.~~, the 95% confidence interval is indicated**

349 **by dash lines.**

350

351 **3.3.3 Tide**

352 The slopes of K_z to internal tide~~s~~al conversion rates represent the mixing response to internal tides. As

353 discussed above, the mixing significantly responded to the internal tides over the entire Philippine Sea

354 (Fig.7). The relationship was depth dependent. The slopes did not reach 0.1 at the depth of 250-500 m,

355 but increased significantly at 500-1000 m and 1000-1500 m. and ~~exceed~~reach 0.1~~28~~3 for the deepest

356 depth band. The response of mixing to internal tides was more significant in the deeper ocean. Focusing

357 on different latitude bands, the slopes of K_z to internal tides is smaller at mid-latitudes. This is because

358 the wind contribution increased in this region, which led to a weakening relative contribution of internal

359 tides. Compared with the internal tide conversion rates, the pattern of K_z was inconsistent with internal

360 tides, even at lower latitudes. It can be inferred that the turbulent mixing was not only affected by the

361 internal tides, but also by other factors. There is a strong western boundary flow, Kuroshio, and an active

362 mesoscale environment in this region. Some researchers have shown that the existence of mesoscale

363 environment will alter the internal tide features, so we reasonably infer that the tidal induced turbulent

364 mixing in this area was modulated by the mesoscale features.

365
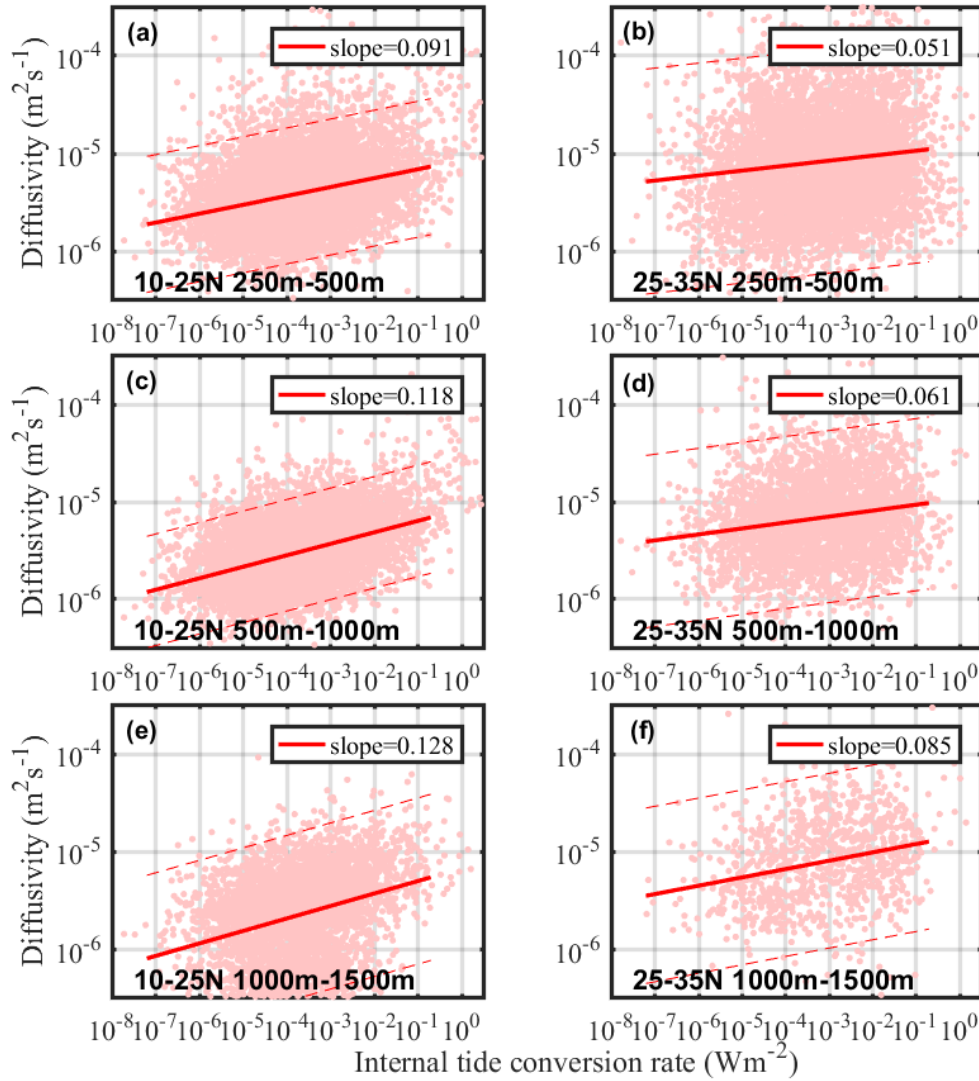
366 **Figure 7 Scatter of log-scale K_z versus log-scale internal tide conversion rate in 250-500 m (row 1), 500-1000**

367 **m (row 2), 1000-15000 m (row 3) and the best-fit slopes are denoted by the red line. Columns 1 and ~~,2,3~~ are**

368 **10°N-~~1~~25°N~~, 15°N -25°N~~ and 25°N -35°N latitude bands, ~~–~~the 95% confidence interval is indicated by dash**

369 **lines.~~respectively.~~**

370

3.4 Role of Mesoscale features in tidal mixing

372 Focusing on the low latitudes, where tidal mixing ~~is~~ dominated, the diapycnal diffusivities, K_z,

373 related to internal tides and eddy kinetic energy are shown ~~in~~ (Fig.8). The combined influences of

374 mesoscale features and internal tides on mixing are indicated. The increasing internal tide conversion

375 rates significantly enhanced turbulent mixing. We find a correlation between elevated eddy kinetic energy

376 and the averaged diapycnal diffusivities for a given internal tide conversion rate level. ~~The increasing~~

377 ~~internal tide conversion rates significantly enhanced turbulent mixing.~~ When the conversion rate was 10^{-}

378 $^3 Wm^{-2}$, the magnitudes of K_z were about $3 \times 10^{-6} m^2 s^{-1}$, $3 \times 10^{-6} m^2 s^{-1}$, $1 \times 10^{-6} m^2 s^{-1}$ at the depth of 250-

379 500 m~~,~~ , 500-1000 m and 1000-1500 m, respectively. When the internal tide conversion rates reached

380 O(-1)-O(0), K_z reached $10^{-5} m^2 s^{-1}$ at both depths of 250-500 m and 500-1000 m, even exceed $10^{-4} m^2 s^{-1}$

381 at some internal tide source sites. In addition, there was a positive correlation between eddy kinetic

382 energy and diapycnal diffusivit~~ies~~y. A higher eddy kinetic energy can further increase K_z under the same

383 magnitude of internal tide conversion rate. Such enhancement was more significant with strong internal

384 tide conversion rates greater than $10^{-3} Wm^{-2}$.

385
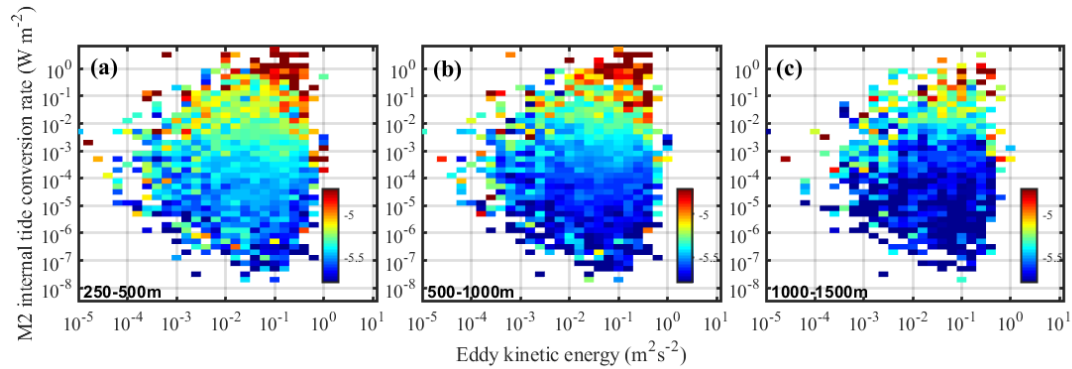
Figure 8 Averaged diapycnal diffusivities as a function of EKE and internal tide conversion rates between (a)
386
387 **250-500 m, (b) 350-500 m and (c) 500-1000 m.**

388

389   M_2 and K_1 tidal constituents were analyzed to clarify the response of K_z to internal tides in the regions

390 of high eddy kinetic energy (EKE is larger than the regional average value) and low eddy kinetic energy

391 (Fig.9). The results integrating 8 main tidal constituents (Fig.9 a, b and c) showed that the slopes in a

392 weak (strong) mesoscale field were smaller (larger), 0.081 (0.105), 0.103(0.134) and 0.103 (0.142) at the

393 depth of 250-500 m, 500-1000 m, 1000-1500 m, respectively. The turbulent mixing was more sensitive

394 to the internal tide magnitude in the presence of an energetic mesoscale field. Moreover, such response

395 was more obvious in the region with strong internal tides (such as $>10^{-2} Wm^{-2}$ conversion rate). In some

396 regions with weak internal tides, such as with internal tide conversion rates less than $10^{-3} Wm^{-2}$, the

397 modulation of mesoscale eddies was less significant.

398
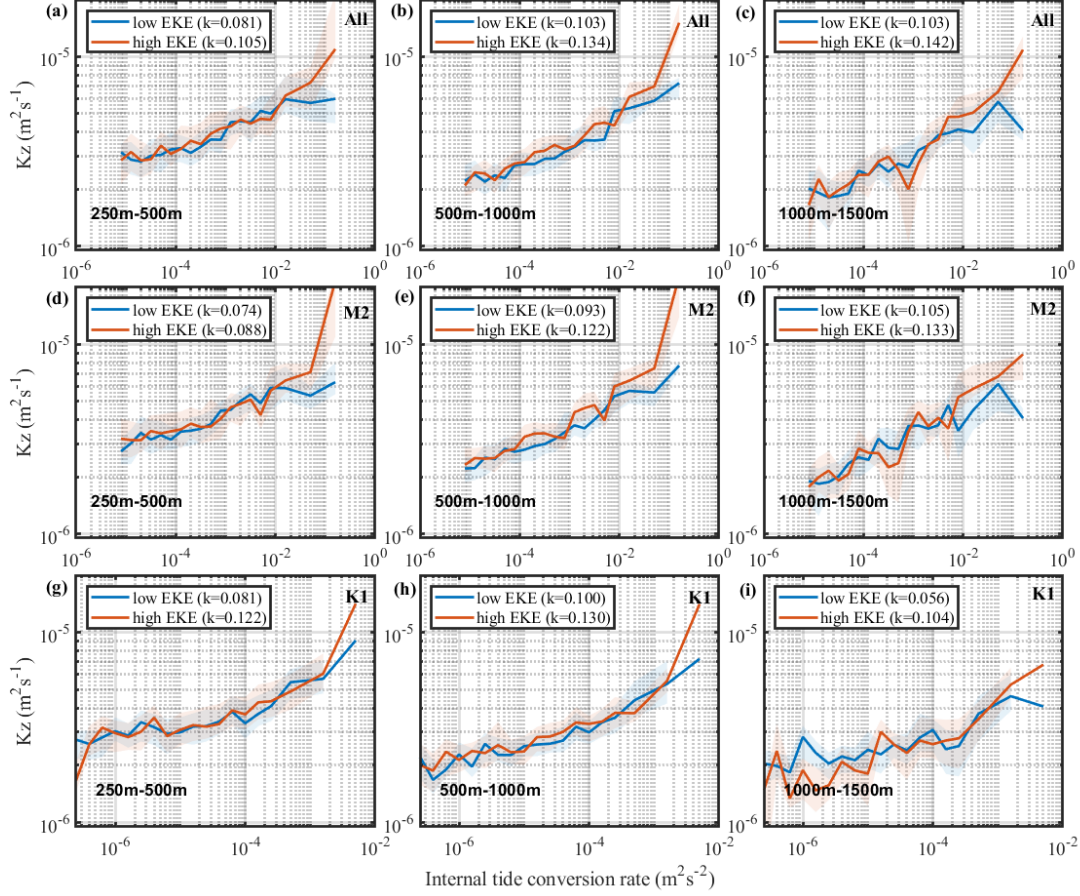
399 **Figure 9 The averaged diffusivity between depths of (a, d, g) 250 m-500 m, (b, e, h) 500 m-1000 m and (c, f, i)**

400 **1000 m-1500 m in high (greater than the median) and low (less than the median) eddy kinetic energy. The**

401 **shade indicate the 1 deviation. Rows 1,2 and 3 are related to 8 main tidal constituents, M_2 internal tide and**

402 **K_1 internal tide, respectively.**

403

404   A similar conclusion can be drawn only considering M_2 or K_1. In regions of high eddy kinetic energy,

405 the change in diffusivities in response to internal tides was significant. And the increase was more

406 sensitive to M_2 internal tide. The enhancement related to M_2 internal tide was more significant below

407 500 m (Fig.9 d and e), while enhancement of the K_1 internal tide was similar at all depths. This may be

408 due to different features and structures of M_2 and K_1 internal tides. In this area, the modal structure and

409 propagation path of M_2 internal tide are more complicated and more prone to breaking, but those of K_1

410 were relatively stable. And this area includes the K_1 critical latitude range, which can be broadened by

411 mesoscale currents (Robertson and Dong, 2019).

412   The modulation of cyclonic and anticyclonic eddies on tidal mixing also differ. The increase of K_z

413 by internal tides in regions with cyclonic eddies (vorticity>$3 \times 10^{-6}s^{-1}$) and anticyclonic eddies

414 (vorticity<-$3 \times 10^{-6}s^{-1}$) are both shown (Fig.10 and Fig.11). Under the same magnitude of internal tides,

the K_z increase more significantly in the presence of anticyclonic eddies, which is obvious in 250-500 m, and can also be seen in 500-1000 m. Below 1000 m, there ~~is~~are no significant differences between the regions with cyclones and anticyclones.
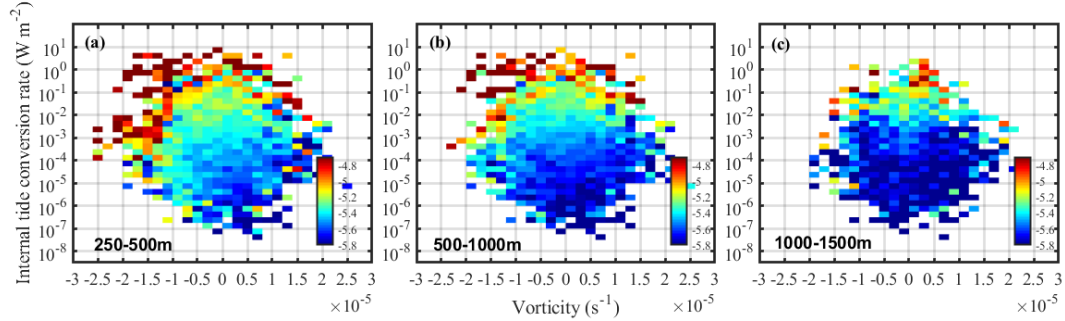
Figure 10 The averaged diapycnal diffusivities as a function of vorticity and internal tides conversion rate between (a) 250-500 m, (b) 500-1000 m and (c) 1000-1500 m

Considering mixing driven by eddies is relatively significant in regions where the tidal mixing is very weak, we only analyze the cases of internal tides conversion rates larger than $10^{-3} Wm^{-2}$. When the conversion rates become larger than this value, the diapycnal diffusivities at the presence of high eddy kinetic energy increase faster with internal tides (Fig. 9). It was found that the response of turbulent mixing to internal tides was more sensitive in the presence of anticyclones above 1000 m. While below 1000 m, the influence of cyclones is slightly ~~higher~~stronger than that of anticyclones.
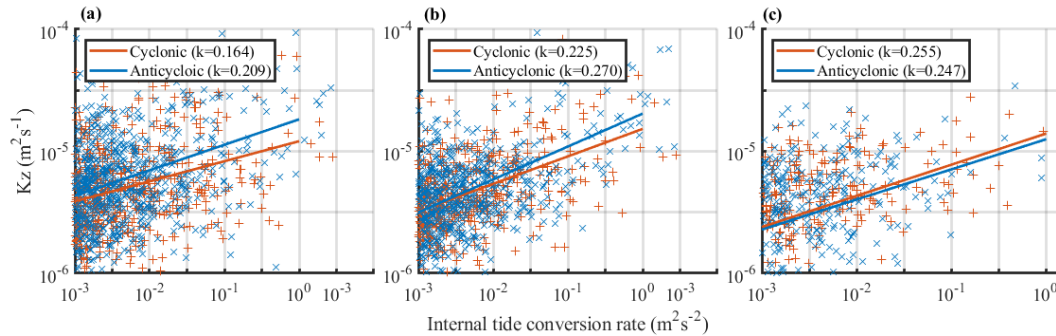
Figure 11 ~~s~~Scatter of log-scale K_z versus log-scale internal tide conversion rate with Cyclone (red) and anticyclone (blue) in (a) 250-500 m, (b) 500-1000 m, and (c) 1000-1500 m. The best-fit slopes are denoted by the red and blue solid line.

4. Summary

The spatial pattern and seasonal variability of the diapycnal diffusivities in the Philippine Sea were estimated using a fine scale parameterization. The main conclusions ~~are as~~ follow~~s~~.

436   The seasonal fluctuations of mixing in this area were zonally dependent. Seasonal variability was

437 strong in winter and weak in summer at mid-latitudes, with the seasonal fluctuations more obvious in the

438 upper ocean. This was attributed to the Westerlies, and the wind plays a more significant role in turbulent

439 mixing here. However, the seasonal cycle of mixing in the low latitudes was not obvious, indicating that

440 the wind-driven mixing was not dominant here. As opposed to wind-driven mixing, tidal mixing was

441 more significant in the deeper ocean.

442   Evidence that the mixing was modulated by internal tides was seen in regions of both high and low

443 eddy kinetic energy, and it was more significant with high eddy kinetic energy. The presence of high

444 eddy kinetic energy enhanced the response of K_z to internal tides, especially for the M_2 internal tide.

445 The increased rate of K_z with internal tides in the high EKE field was higher than that in the weak EKE

446 field. The existence of mesoscale features changed the vertical structure of internal tides, and transferred

447 the internal tides energy from low modes to higher modes. It was more likely to cause internal tide

448 breaking (Dunphy and Lamb 2014). The enhancement by mesoscale motions to tidal mixing was more

449 significant for M_2 internal tides. Anticyclonic eddies were more likely to increase tidal mixing in the

450 upper ocean. While the influence of cyclonic eddies to tidal mixing was slightly higher than that of

451 anticyclonic ones in the deep ocean.

452   There are several mechanisms that might explain the elevated tidal mixing in the present of energetic

453 mesoscale environment. The vertical scales of internal tide can be reduced and the energy of internal tide

454 can be amplified near the surface in the presence of energetic mesoscale features. When internal tide

455 passes through mesoscale eddy, the energy of mode-1 internal tide can be refracted and transmitted to

456 higher-mode waves (eg. Farrari and Wunsch, 2008, Henning and Vallis, 2004). The eddy flows can also

457 directly increase vertical shear and subsequently internal tide energy dissipation rate (eg. Chavanne et

458 al., 2010, Dunphy, 2014). The anticyclones induce higher tidal mixing than do cyclones probably because

459 of the Chimney effects associated with distinct vorticities (Jing and Wu, 2011).

460   This paper explores the modulation of the mesoscale environments on tide-induced mixing statistically

461 through ARGO float observations~~by some observed dataset~~. Theoretical clarification of the driving

462 mechanisms is needed. Some previous numerical studies can explain our conclusion to some extent.

463 However, how and to which extent the vorticity alter internal tide evolution and induced mixing have not

464 been clearly explained in theory. Moreover, the latitude range from 9°N to 36°N are discussed in this

465 work due to the limitations of the fine scale parameterization method in equatorial areas. The influence

466 of the equatorial background flows on ocean mixing remains to be solved.

467

468 **Code and data availability.** The ARGO data (ftp://ftp.argo.org.cn/pub/ARGO/global/) set were made

469 available by China Argo Real-time Data Center (Li Zhaoqin et al., 2019). The near surface 10 m wind

470 speed was product by ERA-Interim dataset (https://www.ecmwf.int/en /forecasts/datasets). The

471 geostrophic velocity were taken from the AVISO (http://www.aviso.altimetry.fr/duacs/). The internal

472 tidal conversion rate was provided by SEANOE (https://www.seanoe.org/data/, C.de Lavergne et al.,

473 2019). The corresponding data and codes are available on request to Zhenhua Xu by email.

474

475 **Author contribution.** The concept of this study was developed by Zhenhua Xu and extended upon by

476 all involved. Jia You implemented the study and performed the analysis with guidance from Zhenhua Xu,

477 Qun Li and Robin Robertson. Peiwen Zhang and Baoshu Yin collaborated in discussing the results and

478 composing the manuscript.

479

480 **Competing interests.** The authors declare that they have no conflict of interest.

481

482 **Acknowledgment.** Funding for this study was provided by the National Key Research and

483 Development Program of China (No. 2016YFC1402705, 2017YFA0604102), the Strategic Priority

484 Research Program of Chinese Academy of Sciences (No.XDB42000000, XDA11010204), the National

485 Natural Science Foundation of China (91858103, 41676006), Key Research Program of Frontier

486 Sciences, CAS.

487 **References**

488 Alford, M. H., and Gregg, M. C.: Near‑inertial mixing: Modulation of shear, strain and microstructure
489   at low latitude, J. Geophys. Res., 106(C8), 16947– 16968, 2001.
490 Alford, M. H.: Improved global maps and 54-year history of wind-work on ocean inertial motions.
491   Geophys. Res. Lett., 30,1424, 2003.
492 Alford, M. H., MacKinnon, J. A., Simmons, H. L. & Nash, J. D.: Near-inertial internal gravity waves in
493   the ocean. Annu. Rev. Mar. Sci. 8, 95–123, 2016.
494 Ansong, J.K., B.K. Arbic, H.L. Simmons, M.H. Alford, M.C. Buijsman, P.G. Timko, J.G. Richman, J.F.
495   Shriver, and A.J. Wallcraft: Geographical Distribution of Diurnal and Semidiurnal Parametric
496   Subharmonic Instability in a Global Ocean Circulation Model. J. Phys. Oceanogr., 48, 1409–1431,
497   2018.

Cao, Anzhou & Guo, Zheng & Song, Jinbao & Lv, Xianqing & He, Hailun & Fan, Wei. (2018). Near-Inertial Waves and Their Underlying Mechanisms Based on the South China Sea Internal Wave Experiment (2010-2011). Journal of Geophysical Research: Oceans. 123. 10.1029/2018JC013753.

Chang, H., Xu, Z., Yin, B., Hou, Y., Liu,Y., Li, D., et al.: Generation and propagation of M2 internal tides modulated by the Kuroshio northeast of Taiwan. Journal of Geophysical Research: Oceans, 124, 2728－2749, 2019.

Chavanne, C., Flament, P., Luther, D., & Gurgel, K. W.: The surface expression of semidiurnal internal tides near a strong source at Hawaii. Part Ⅱ: interactions with mesoscale currents*. JOURNAL OF PHYSICAL OCEANOGRAPHY, 40(6), 1180-1200, 2010.

Deepwell, D., Stastna, M., Carr, M., and Davis, P. A., (2017), Interaction of a mode-2 internal solitary wave with narrow isolated topography, Physics of Fluid, 29, 076601. https://doi.org/10.1063/1.4994590

Dong, J., R. Robertson, C. Dong, P. S. Hartlipp, T. Zhou, Z. Shao, W. Lin, M. Zhou, and J. Chen: Impacts of mesoscale currents on the diurnal critical latitude dependence of internal tides: A numerical experiment based on Barcoo Seamount, J. Geophys. Res. Oceans, 2019.

Dunphy, M., and K. G. Lamb: Focusing and vertical mode scattering of the fifirst mode internal tide by mesoscale eddy interaction. J. Geophys. Res. Oceans, 119, 523–536, 2014.

Egbert, G. D., and R. D. Ray: Estimates of M2 tidal energy dissipation from TOPEX/Poseidon altimeter data. J. Geophys. Res., 106, 22 475–22 502, 2001.

Fer, I., Skogseth, R., & Geyer, F.: Internal waves and mixing in the marginal ice zone near the yermak plateau *. Journal of Physical Oceanography, 40(7), 1613-1630, 2010.

Ferrari, R., and C. Wunsch: Ocean circulation kinetic energy: Reservoirs, sources, and sinks. Annu. Rev. FluidMech., 41, 253, 2009.

Grimshaw, R., Pelinovsky, E., Talipova, T., & Kurkina, O.: Internal solitary waves: propagation, defor mation and disintegration. Nonlinear Processes in Geophysics, 17(6), 633-649.

Huang, X., Wang, Z. , Zhang, Z. , Yang, Y. , Zhou, C. , & Yang, Q. , et al.: Role of mesoscale eddies in modulating the semidiurnal internal tide: observation results in the northern south china sea. Journal of Physical Oceanography, 48(8), 1749-1770, 2018.

Jayne, S. R., and L. C. St. Laurent: Parameterizing tidal dissipation over rough topography. Geophys. Res. Lett., 28, 811–814, 2001.

Jeon, C., Park, J.－H., & Park, Y.－G.: Temporal and spatial variability of near－inertial waves in the East/Japan Sea from a high－resolution wind－forced ocean model. Journal of Geophysical Research: Oceans, 124, 6015–6029, 2018. https://doi.org/10.1029/2018JC014802

Jing, Z., Wu, L., Li, L., Liu, C , Liang, X., & Chen, Z., et al.: Turbulent diapycnal mixing in the subtropical northwestern pacific: spatial-seasonal variations and role of eddies. Journal of Geophysical Research Oceans, 116., 2011.

Jing, Z. & Wu, L.: Intensified diapycnal mixing in the mid-latitude western boundary currents. Rep, 4(1), 7412, 2014.

Kerry, C. G., Powell, B. S., & Carter, G. S.: Effects of remote generation sites on model estimates ofM2 internal tides in the Philippine Sea. Journal of Physical Oceanography, 43(1), 187－204, 2013.

Kerry, C.G., B.S. Powell, and G. S. Carter: The impact of subtidal circulation on internal tide generation and propagation in the Philippine Sea. J. Phys. Oceanogr., 44, 1386–1405, 2014.

Kerry, C. G., Powell, B. S., & Carter, G. S.: Quantifying the incoherent m 2 internal tide in the Philippine sea. Journal of Physical Oceanography, 46(8), 2483-2491, 2016.

542 Klymak, J.M., J.N. Moum, J.D. Nash, E. Kunze, J.B. Girton, G.S. Carter, C.M. Lee, T.B. Sanford, and
543   M.C. Gregg: An Estimate of Tidal Energy Lost to Turbulence at the Hawaiian Ridge. J. Phys.
544   Oceanogr., 36, 1148–1164, 2006.

545 Kunze, E.: Internal-wave-driven mixing: global geography and budgets. Journal of Physical
546   Oceanography, JPO-D-16-0141.1, 2017.

547 Liu A K, Su F C, Hsu M K et al.: Generation and evolution of mode-two internal waves in the South
548   China Sea. Cont. Shelf Res., 59:18-27, http://dx.doi.org/10.1016/j.csr.2013.02.009, 2013.

549 Liu, G., W. Perrie, and C. Hughes: Surface wave effects on the wind-power input to mixed layer near-
550   inertial motions. J. Phys. Oceanogr., 47, 1077–1093, 2017.

551 Li Zhaoqin, Liu Zenghong, Xing Xiaogang: User Manual for Global Argo Observational data set (V3.0)
552   (1997-2019), China Argo Real-time Data Center, Hangzhou, 37pp, 2019.

553 MacKinnon, J. A. et al.: Climate process team on internal-wave driven ocean mixing. Bull. Am. Meteorol.
554   Soc. 98, 2429–2454, 2017.

555 Munk, W., and C. Wunsch: Abyssal recipes II: Energetics of tidal and wind mixing. Deep-Sea Res. I, 45,
556   1977–2010, 1998.

557 Muller, M.: On the space‐ and time‐dependence of barotropic‐to‐baroclinic tidal energy
558   conversion. Ocean Modelling, 72, 242–252, 2013.

559 Nagasawa, M., Hibiya, T., Furuichi, N. et al.: Temporal Variability of High Vertical Wavenumber Shear
560   over the Izu-Ogasawara Ridge. J Oceanogr 61, 1101–1105, 2005.

561 Nash, J. D., E. L. Shroyer, S. M. Kelly, and M. E. Inall: Are any coastal internal tides predictable?
562   Oceanography, 25 (2), 80–95, 2012.

563 Park, J.-H., and D. R. Watts: Internal tides in the southwestern Japan/East Sea. J. Phys. Oceanogr., 36,
564   22–34, 2006.

565 Ponte, A. L., and P. Klein: Incoherent signature of internal tides on sea level in idealized numerical
566   simulations. 1769Geophys. Res. Lett., 42, 1520–1526, 2015.

567 Qiu, B., Chen, S., and Carter, G. S.: Time‐varying parametric subharmonic instability from repeat CTD
568   surveys in the northwestern Pacific Ocean, J. Geophys. Res., 117, C09012, 2012.

569 Rainville, L., & Pinkel, R.: Propagation of low-mode internal waves through the ocean. Journal of
570   Physical Oceanography, 36(6), p.1220-1236, 2006.

571 Rimac, A., J.-S. von Storch, C. Eden, and H. Haak: The influence of high resolution wind stress field on
572   the power input to near-inertial motions in the ocean. Geophys. Res. Lett., 40,4882–4886 , 2013.

573 Robertson, R.: Internal tides and baroclinicity in the southern Weddell Sea: 1. Model description.
574   Journal of Geophysical Research, 27001-27016, https://doi.org/10.1029/2000JC000475, 2001.

575 Robertson, R., and C M. Dong: An evaluation of the performance of vertical mixing parameterizations
576   for tidal mixing in the Regional Ocean Modeling System (ROMS), Geoscience Letters, 6 (15), 2019.

577 Shen, H., Perrie, W., & Johnson, C. L.: Predicting internal solitary waves in the gulf of maine. Journal
578   of Geophysical Research: Oceans, 125(3), 2020.

579 Song, P., and X. Chen.: Investigation of the Internal Tides in the Northwest Pacific Ocean Considering t
580   he Background Circulation and Stratification. J. Phys. Oceanogr., 50, 3165–3188,
581   2020. https://doi.org/10.1175/JPO-D-19-0177.1.

582 Tanaka, T., Hasegawa, D., Yasuda, I., Tsuji, H., Fujio, S., & Goto, Y., et al.: Enhanced vertical turbulent
583   nitrate flux in the kuroshio across the izu ridge. Journal of Oceanography, 1-9, 2018.

584 Vlasenko, V., Stashchuk, N., Palmer, M. R., & Inall, M. E.: Generation of baroclinic tides over an
585   isolated underwater bank. Journal of Geophysical Research Oceans, 118(9), 2013.

586   https://doi.org/10.1002/jgrc.20304

587   Watanabe, M., and T. Hibiya: Global estimates of the wind induced energy flux to inertial motions in the

588   surface mixed layer. Geophys. Res. Lett., 29, 1239, 2002.

589   Wang, Y., Xu, Z., Yin, B., Hou, Y., & Chang, H.: Long‐range radiation and interference pattern of

590   multisource M2 internal tides in the Philippine Sea. Journal of Geophysical Research:

591   Oceans, 123, 5091– 5112, 2018.

592   Waterhouse, A.F., J.A. MacKinnon, J.D. Nash, M.H. Alford, E. Kunze, H.L. Simmons, K.L. Polzin, L.C.

593   St. Laurent, O.M. Sun, R. Pinkel, L.D. Talley, C.B. Whalen, T.N. Huussen, G.S. Carter, I. Fer, S.

594   Waterman, A.C. Naveira Garabato, T.B. Sanford, and C.M. Lee: Global Patterns of Diapycnal

595   Mixing from Measurements of the Turbulent Dissipation Rate. J. Phys. Oceanogr., 44, 1854–1872,

596   2014.

597   Whalen, C. B., Talley, L. D., & Mackinnon, J. A.: Spatial and temporal variability of global ocean mixing

598   inferred from ARGO profiles. Geophysical Research Letters, 39(18), 2012.

599   Whalen, C.B., MacKinnon, J.A. & Talley, L.D.: Large-scale impacts of the mesoscale environment on

600   mixing from wind-driven internal waves.Nature Geosci 11, 842–847, 2018.

601   Wu, L. , Jing, Z. , Riser, S. , & Visbeck, M.: Seasonal and spatial variations of southern ocean diapycnal

602   mixing from argo profiling floats. Nature Geoscience, 2011.

603   Wunsch, C., and R. Ferrari: Vertical mixing, energy and the general circulation of the oceans. Annu. Rev.

604   Fluid Mech., 36, 281–314, 2004.

605   Xu, Z., Liu, K., Yin, B., Zhao, Z., Wang, Y., & Li, Q.: Long-range propagation and associated

606   variability of internal tides in the South China Sea, Journal of Geophysical Research: Oceans, 121,

607   8268–8286, 2016.

608   Xu, Z., Yin, B., Hou, Y., & Liu, A. K.: Seasonal variability and north–south asymmetry of internal

609   tides in the deep basin west of the Luzon Strait, Journal of Marine Systems, 134, 101–112, 2014.

610   Xu, Z., Yin, B., Hou, Y., & Xu, Y.: Variability of internal tides and near-inertial waves on the

611   continental slope of the northwestern South China Sea, Journal of Geophysical Research: Oceans,

612   118, 197–211, 2013.

613   Zhang, Z., Qiu, B., Tian, J. et al.: Latitude-dependent finescale turbulent shear generations in the Pacific

614   tropical-extratropical upper ocean.Nat Commun 9, 4086, 2018.

615   Zhao,Z., M. H. Alford, J. A. MacKinnon, and R. Pinkel: Long-range propagation of the semidiurnal

616   internal tide from the Hawaiian Ridge. J. Phys. Oceanogr., 40, 713–736, 2010.

617   Zhao, Z.: Mapping internal tides from satellite altimetry without blind directions. Journal of

618   Geophysical Research: Oceans, 124, 2019. https://doi.org/10.1029/2019JC015507

619

620